Eurasian Chemico-Technological Journal 16 (2014) 227-238

Transported Joint Probability Density Function Modeling of Turbulent Dilute Spray Flows

Y. Hu and E. Gutheil*

Interdisciplinary Center for Scientific Computing, University of Heidelberg, 69120 Heidelberg, Germany

Abstract

A transported joint probability density function (PDF) model for turbulent spray flows is presented, where a one-point one-time statistical description of the gas-phase mixture fraction and the gas velocity is used. This approach requires the closure of the molecular mixing, which is achieved through use of the extended interaction-by-exchange-with-the-mean (IEM) model and a simplified Langevin model for the closure of the gas velocity both of which are extended through additional terms accounting for spray evaporation. These equations require the solution of the turbulent time scales and the mean pressure field through a Eulerian description. The numerical approach includes a Lagrangian Monte Carlo method for the solution of modeled joint PDF equation with a Eulerian finite-volume algorithm to determine the turbulent time scale and the mean pressure field. For the dispersed liquid phase, Lagrangian equations are used to describe the droplet heating, evaporation, and motion in the framework of a discrete droplet model. The convective droplet evaporation model is employed, and the infinite conductivity model with consideration of non-equilibrium effects based on the Langmuir-Knudsen law is used. The droplet turbulent dispersion is modeled with two different Lagrangian stochastic models. The resulting spray evolution equations are solved by a Lagrangian discrete droplet method using the point source approximation for a dilute spray. The numerical results are compared with experimental data of Gounder et al. [1], where the experimental set B of the acetone spray flows SP2 and SP6 are simulated. Comparison of numerical and experimental results includes droplet size, liquid volume flux as well as the mean and fluctuating velocities. Generally, good agreement is achieved, although the radial droplet dispersion is somewhat under-predicted by the computations. The droplet fluctuating velocities show sensitivity to the different dispersion models.

Introduction

Many industrial applications operate with liquid fuels, for instance devices for power generation, where the fuel is sprayed into a chamber, followed by a number of interacting processes, i.e., droplet dispersion, evaporation, turbulent mixing and combustion. The complexity involved in these gas-liquid two-phase flows is tremendous, and the strong interactions between spray, turbulence, and chemistry in a broad range of time and length scales present a great challenge for modeling and simulation of these spray processes. Popular approaches include direct numerical simulation (DNS), large eddy simulation (LES), and Reynolds-averaged Navier-Stokes (RANS) equation modeling. In DNS, all scales are resolved, which is not affordable for realistic technical applications. RANS and LES are useful tools in industrial applications at reasonable computational cost, although the sub-grid scale (SGS) modeling raises open issues for complex multi-phase flows in LES [2]. The probability density function (PDF) method provides a suitable approach to couple the spray evaporation to the turbulent flow field, since it can account for the turbulent fluctuations of the fluid variables considered, and the local PDF of scalars is well represented in the presence of evaporating droplets [3], which is of crucial importance in reactive sprays.

Improving mathematical and numerical models is a difficult task, and it is usually assisted by careful comparison with simple but representative experiment. Guided by the success of the Turbulent Nonpremixed Flames (TNF) workshop series (www.sandia.gov/TNF), the workshop series Measurement and Computation of Turbulent Spray Combustion (www.tcs-workshop.org) was initiated in 2009, and it aims at advancing current understanding of

* Corresponding author. E-mail: gutheil@iwr.uni-heidelberg.de

the underlying physical-chemical processes in both non-reacting and reacting spray flows [4]. In this framework, a series of comprehensive dilute spray jets and flames with different characteristics of turbulence, droplet mass loading and fuel type have been studied experimentally [1, 5]. Many excellent studies attributed to the computational studies of these test sprays have been reported [6-8]. Chrigui et al. [6] studied reacting acetone sprays [1] using an LES approach with a discrete spray model and Flamelet Generated Manifold (FGM) tabulated chemistry. The computed results of droplet size, mass flux and gas temperature were compared with the experiments. In this approach, the effect of the sub-grid scale dispersion on evaporating droplets is neglected, which could possibly improve the computational results. A numerical investigation of reacting ethanol sprays with LES is also performed by De et al. [7], where the turbulence-chemistry interaction is described with a flamelet-progress variable (FPV), where the sub-filter fluctuations of the gas temperature and the composition seen by the droplets along the trajectory are taken into account. These results [7] suggest that in the present dilute reacting sprays, the effects of SGS scalar fluctuation on droplet evaporation depend on the liquid mass flow rate and the amount of pre-vaporized liquid at the inlet. Heye et al. [8] combined a joint mixture fraction and process variable PDF with LES of a turbulent ethanol spray flame, and a Lagrangian Monte-Carlo algorithm for solving the modeled PDF transport equation was used.

In the present study, following the Eulerian-Lagrangian approach, a joint PDF of the mixture fraction and the gas velocity is used, where the molecular mixing is described with an extended interaction-by-exchange-with-the-mean (IEM) model, and the particle evolution equation is closed with an extended simplified Langevin model [9, 10]. The extension concerns additional terms to account for droplet evaporation. The dilute spray model includes the description of the convective droplet heating, evaporation, and motion. A non-equilibrium evaporation model is used to account for the thermodynamic non-equilibrium effect at the droplet surface. Two different turbulent droplet dispersion models are implemented and evaluated. The numerical results are compared with the experimental set B by Masri et al. [5] for two test cases (SP2 and SP6), where two poly-disperse turbulent acetone spray flows with different initial liquid mass load were studied.

Mathematical Modeling

In this section, the mathematical models for both the carrier gas and the dispersed liquid phase are presented. The transported joint PDF for the gas velocity and the mixture fraction is modeled and solved, and a discrete Lagrangian description is used for the evolution of the dispersed droplets assuming a dilute spray.

Gas Phase

In both non-reacting and reacting spray flows, the momentum and the turbulent mixing in the gas phase are crucial for the evolution of dispersed droplets and the characteristics of the gas, which motivates the choice of a statistical description of a joint gas velocity - mixture fraction probability density function model for the gas phase [9]. The definition of the mixture fraction is based on the chemical element C [3, 11]. With the definition of a fine-grained, one-point one-time Eulerian joint gas velocity - mixture fraction probability density function f^* (V, ζ; x, t) for the gas phase of turbulent spray flows [9]

$$\boldsymbol{f}^*(\mathbf{V},\boldsymbol{\zeta};\mathbf{x},\boldsymbol{t}) = \boldsymbol{\delta}(\mathbf{U}(\mathbf{x},\boldsymbol{t})-\mathbf{V})\boldsymbol{\delta}(\boldsymbol{\xi}(\mathbf{x},\boldsymbol{t})-\boldsymbol{\zeta}), \quad (1)$$

where V and ζ are the sample space variables of the gas velocity, U (x, t) and the mixture fraction, ξ, respectively.

The transport equation of the mass density function $F(\mathbf{V},\zeta;\mathbf{x},t) = \langle\rho\rangle\tilde{f}(\mathbf{V},\zeta;\mathbf{x},t)$ with dependent variables gas velocity and mixture fraction yields [9]

$$\frac{\partial \boldsymbol{F}}{\partial \boldsymbol{t}} + \frac{\partial (\boldsymbol{V}_i \boldsymbol{F})}{\partial \boldsymbol{x}_i} - \frac{\langle \boldsymbol{S}_\mathrm{v}\rangle}{\langle\boldsymbol{\rho}\rangle} + \frac{\mathbf{1}}{\langle\boldsymbol{\rho}\rangle}\langle(\mathbf{1}-\boldsymbol{\xi})\boldsymbol{S}_\mathrm{v}\rangle\frac{\partial \boldsymbol{F}}{\partial \boldsymbol{\zeta}} \quad (2)$$

$$+\left(\boldsymbol{g}_i - \frac{\mathbf{1}}{\langle\boldsymbol{\rho}\rangle}\frac{\partial\langle \boldsymbol{p}\rangle}{\partial \boldsymbol{x}_i} + \frac{\mathbf{1}}{\langle\boldsymbol{\rho}\rangle}\langle \boldsymbol{S}_{\mathrm{m},i} - \boldsymbol{U}_i\boldsymbol{S}_\mathrm{v}\rangle\right)\frac{\partial \boldsymbol{F}}{\partial \boldsymbol{V}_i} = \left\langle \frac{\boldsymbol{S}'_\mathrm{v}}{\boldsymbol{\rho}}\middle|\mathbf{V},\boldsymbol{\zeta}\right\rangle \boldsymbol{F}$$

$$+\frac{\partial}{\partial \boldsymbol{V}_i}\left(\frac{\mathbf{1}}{\langle\boldsymbol{\rho}\rangle}\left\langle -\frac{\partial \boldsymbol{\tau}_{ij}}{\partial \boldsymbol{x}_j} + \frac{\partial \boldsymbol{p}'}{\partial \boldsymbol{x}_i} - \boldsymbol{S}'_{\mathrm{m},i} + [\boldsymbol{U}_i\boldsymbol{S}_\mathrm{v} - \langle \boldsymbol{U}_i\boldsymbol{S}_\mathrm{v}\rangle]\middle|\mathbf{V},\boldsymbol{\zeta}\right\rangle \boldsymbol{F}\right)$$

$$-\frac{\partial}{\partial \boldsymbol{\zeta}}\left(\frac{\mathbf{1}}{\langle\boldsymbol{\rho}\rangle}\left\langle \frac{\partial}{\partial \boldsymbol{x}_j}\left(\boldsymbol{\rho}\boldsymbol{D}_M\frac{\partial \boldsymbol{\xi}}{\partial \boldsymbol{x}_j}\right) + [(\mathbf{1}-\boldsymbol{\xi})\boldsymbol{S}_\mathrm{v} - \langle(\mathbf{1}-\boldsymbol{\xi})\boldsymbol{S}_\mathrm{v}\rangle]\middle|\mathbf{V},\boldsymbol{\zeta}\right\rangle \boldsymbol{F}\right).$$

Here, τ_{ij} is the viscous stress tensor, p the local pressure field, and S_v and $S_{\mathrm{m},i}$ are the spray source terms for the transfer of mass and momentum between the liquid and gas phases, respectively, which will be given in the next section. In Eq. (2), the terms on the right hand side are unclosed and require modeling. They represent the effect of fluctuating spray source terms, which are neglected in the present work, and transport in gas velocity and mixture fraction space due to the molecular processes and the fluctuating pressure.

For the solution of this high dimensional equation, a stochastic Lagrangian Monte-Carlo method is suitable [12]. Thus, the mass density function, F, is computed from an ensemble of notional stochastic particles with a set of properties, (m^*, x^*, U^*, ξ^*). The joint PDF transport equation is then transformed into a set of stochastic differential equations (SDEs), which provides the evolution of each particle and its properties. The time evolution of the gas particle velocity is determined by the extended simplified Langevin model [12]

$$\mathrm{d}U_i^*(t) = \left(g_i - \frac{1}{\langle\rho\rangle}\frac{\partial\langle p\rangle}{\partial x_i} + \frac{1}{\langle\rho\rangle}\left(\langle S_{\mathrm{m},i}\rangle - \langle U_i\rangle\langle S_{\mathrm{v}}\rangle\right)\right)\mathrm{d}t - \left(\frac{1}{2}+\frac{3}{4}C_0\right)\left(U_i^*(t) - \langle U_i\rangle\right)\frac{\tilde{\varepsilon}}{\tilde{k}}\mathrm{d}t + \sqrt{C_0\tilde{\varepsilon}}\,\mathrm{d}W_i. \quad (3)$$

Here, the diffusion process is represented by the increment of the Wiener process dW_i, which follows a Gaussian distribution with $\langle \mathrm{d}W_i(t)\rangle = 0$ and $\langle \mathrm{d}W_i(t)\mathrm{d}W_j(t)\rangle = \mathrm{d}t\delta_{ij}$. The linear drift term includes the body force, mean pressure gradients, and the spray source terms that represent the force exerted by the liquid droplets.

The molecular diffusion is described through use of the interaction-by-exchange-with-the-mean (IEM) model, which is extended to account of the spray evaporation [9, 13]

$$\frac{\mathrm{d}\xi^*(t)}{\mathrm{d}t} = -\frac{1}{2}\frac{\tilde{\varepsilon}}{\tilde{k}}C_\phi\left[\xi^*(t) - \langle\xi\rangle\right] + \left[1 - \langle\xi\rangle\right]\frac{\langle S_{\mathrm{v}}\rangle}{\langle\rho\rangle}. \quad (4)$$

In Eqs. (3) and (4), $\langle U_i\rangle$ and $\langle\xi\rangle$ represent the estimated mean velocity and mixture fraction, respectively. $\tilde{k}$ and $\tilde{\varepsilon}$ denote the turbulent kinetic energy and its dissipation rate, and the standard constants $C_0 = 2.1$, $C_\phi = 2.0$ are used [9].

For the closure of the joint PDF transport equation, the Favre-averaged conservation equations of mass, momentum and enthalpy of the gas phase in the turbulent spray flow are required. They include source terms, S_{v}, $S_{\mathrm{m},i}$, and S_{e}, to describe the exchange between the gas and the liquid phases [11]

$$\frac{\partial\bar{\rho}}{\partial t} + \frac{\partial(\bar{\rho}\tilde{U}_j)}{\partial x_j} = \bar{S}_{\mathrm{v}} \quad (5)$$

$$\frac{\partial(\bar{\rho}\tilde{U}_i)}{\partial t} + \frac{\partial(\bar{\rho}\tilde{U}_j\tilde{U}_i)}{\partial x_j} - \frac{\partial}{\partial x_j}\left(\Gamma_{\tilde{U}_i,\mathrm{eff}}\frac{\partial\tilde{U}_i}{\partial x_j}\right) = -\frac{\partial\bar{p}}{\partial x_i} - \frac{\partial}{\partial x_i}\left(\frac{2}{3}\Gamma_{\tilde{U}_i,\mathrm{eff}}\frac{\partial\tilde{U}_k}{\partial x_k}\right) + \bar{\rho}g_i + \bar{S}_{\mathrm{m},i} \quad (6)$$

$$\frac{\partial(\bar{\rho}\tilde{h})}{\partial t} + \frac{\partial(\bar{\rho}\tilde{U}_j\tilde{h})}{\partial x_j} - \frac{\partial}{\partial x_j}\left(\Gamma_{\tilde{h}_i,\mathrm{eff}}\frac{\partial\tilde{h}}{\partial x_j}\right) = \frac{\partial\bar{p}}{\partial t} + \bar{S}_{\mathrm{e}}. \quad (7)$$

Here, the viscosity hypothesis for turbulent fluxes of mass, momentum, and enthalpy is used, and $\Gamma_{\tilde{\Phi},\mathrm{eff}} = \eta_l/\sigma_{\Phi,l} + \eta_t/\sigma_{\Phi,t}$ denotes the effective exchange coefficient for variable Φ. $\sigma_{\Phi,l}$ and $\sigma_{\Phi,t}$ are the laminar and turbulent Prandtl-Schmidt numbers, respectively, and η_l and η_t are the molecular and turbulent dynamic viscosities, respectively, $\eta_t = C_\eta\bar{\rho}\tilde{k}^2/\tilde{\varepsilon}$ where with C_η= 0.09. $\tilde{k}$ and $\tilde{\varepsilon}$ denote the turbulent kinetic energy and its dissipation rate, and they are obtained by solving an extended k-ε model [11]. The transport equations for $\tilde{k}$ and $\tilde{\varepsilon}$ yield [11]

$$\frac{\partial(\bar{\rho}\tilde{k})}{\partial t} + \frac{\partial(\bar{\rho}\tilde{U}_j\tilde{k})}{\partial x_j} - \frac{\partial}{\partial x_j}\left(\Gamma_{\tilde{k},\mathrm{eff}}\frac{\partial\tilde{k}}{\partial x_j}\right) = G_k - \bar{\rho}\tilde{\varepsilon} - \frac{2}{3}\bar{\rho}\tilde{k}\frac{\partial\tilde{U}_j}{\partial x_j} + \bar{S}_k \quad (8)$$

and

$$\frac{\partial(\bar{\rho}\tilde{\varepsilon})}{\partial t} + \frac{\partial(\bar{\rho}\tilde{U}_j\tilde{\varepsilon})}{\partial x_j} - \frac{\partial}{\partial x_j}\left(\Gamma_{\tilde{\varepsilon},\mathrm{eff}}\frac{\partial\tilde{\varepsilon}}{\partial x_j}\right) = \left(C_{\varepsilon1}G_k - C_{\varepsilon2}\bar{\rho}\tilde{\varepsilon}\right)\frac{\tilde{\varepsilon}}{\tilde{k}} - \left(\frac{2}{3}C_{\varepsilon1} - C_{\varepsilon3}\right)\bar{\rho}\tilde{\varepsilon}\frac{\partial\tilde{U}_j}{\partial x_j} + \bar{S}_\varepsilon, \quad (9)$$

where the production term, G_k of $\tilde{k}$ is given as

$$G_k = \eta_t\left\{\left(\frac{\partial\tilde{U}_j}{\partial x_i} + \frac{\partial\tilde{U}_i}{\partial x_j}\right) - \frac{2}{3}\left(\frac{\partial\tilde{U}_k}{\partial x_k}\right)\delta_{ij}\right\}\frac{\partial\tilde{U}_i}{\partial x_j}. \quad (10)$$

In the above equations, $\bar{S}_k$ is the spray source term for the turbulent kinetic energy $\tilde{k}$, and $\bar{S}_\varepsilon = c_S\frac{\tilde{\varepsilon}}{\tilde{k}}\bar{S}_k$ is the source term for the turbulent kinetic dissipation rate [11]. The model constants are $C_{\varepsilon1}$ = 1.44, $C_{\varepsilon2}$ = 1.92, $C_{\varepsilon3}$ = -1.0, and c_S = 1.5 [11].

Liquid Phase

The point source approximation is assumed for the poly-disperse spray, and spherically symmetric droplets are considered. Since the density of the liquid is much larger than that of the carrier gas, $\rho_l \gg \langle\rho\rangle$, the forces considered for droplet motion include the drag and gravity, and the velocity, $V_{\mathrm{d},i}$ in i direction is described as

$$\frac{dV_{\mathrm{d},i}}{dt} = \frac{3}{8}\frac{1}{r_{\mathrm{d}}}\frac{\langle\rho\rangle}{\rho_l}C_D\left(U_i - V_{\mathrm{d},i}\right)\left|U_i - V_{\mathrm{d},i}\right| + g_i, \quad (11)$$

where r_d is the droplet radius and g_i the gravitational acceleration. $U_i = \tilde{U}_i + u_i''$ is the instantaneous gas velocity in the i direction seen by the droplet along its trajectory. Following the correlation given by Schiller and Naumann [14], the drag coefficient, C_D, based on the droplet Reynolds number $\mathrm{Re_d} = 2r_d\rho|\mathrm{u} - \mathrm{v_d}|/\mu_\mathrm{f}$ where μ_f is the mean dynamic viscosity in the film, is determined from [14]

$$C_D = \begin{cases} \frac{24}{\mathrm{Re_d}}\left(1 + 0.15\mathrm{Re_d^{0.687}}\right) & \text{if } \mathrm{Re_d} \le 10^3 \\ 0.44 & \text{if } \mathrm{Re_d} > 10^3 \end{cases}. \quad (12)$$

Using Eq. (11), the droplet stochastic positions, $x_{\mathrm{d},i}$, in the flow domain are updated following

$$\frac{dx_{\mathrm{d},i}}{dt} = V_{\mathrm{d},i}. \quad (13)$$

During the Lagrangian tracking procedure, the local instantaneous gas velocity U_i has to be determined, which reflects the effect of turbulence on droplet dispersion. The mean gas velocity $\tilde{U}_i$ can be estimated using the droplet position from the neighboring mean fluid velocity at the grid-point, whereas the fluid fluctuation part u_i'' still requires modeling. In the present study, two different stochastic closure approaches are used and evaluated.

One of the commonly used approaches is the so-called eddy-life time model proposed by Gosman and Ioannides [15]. This model makes use of the concept of droplet-eddy interactions, and assumes that the droplets interact with a sequence of turbulent eddies. Within one droplet-eddy interaction time, τ_{corr}, the fluid velocity experienced by the droplet remains constant, and the fluctuating velocity is sampled from a Gaussian distribution with expected value of zero and a standard deviation of $\sqrt{2\tilde{k}/3}$, which yields

$$f(\mathrm{u}'') = \left(\frac{4\pi}{3}\tilde{k}\right)^{-\frac{1}{2}} \exp\left(-\frac{3}{4\tilde{k}}\mathrm{u}''^2\right). \quad (14)$$

The interaction time, τ_{tt} of the droplet with a certain eddy is determined by taking the minimum value of the eddy life-time, $\tau_{\mathrm{lt}} = L_{\mathrm{te}}/\sqrt{2\tilde{k}/3}$ and the eddy transit time, $\tau_{\mathrm{tt}} = L_{\mathrm{te}}/|\mathrm{u} - \mathrm{v_d}|$, as

$$\tau_{\mathrm{corr}} = \min(\tau_{\mathrm{lt}}, \tau_{\mathrm{tt}}). \quad (15)$$

The characteristic length scale of turbulent eddy is estimated as $L_{\mathrm{te}} = C_\mu^{3/4}\tilde{k}^{3/2}/\tilde{\varepsilon}$ with constant C_μ = 0.09 [15].

Another droplet dispersion model considered here is the single-step Langevin equation model [16]. In this model, the fluctuating velocities at two successive time steps are correlated according to the following Langevin equation [16]

$$u_i''(t_{n+1}) = R_{P,i}(\Delta t, \Delta r)u_i''(t_n) + \sigma\chi_i\sqrt{1 - R_{P,i}^2(\Delta t, \Delta r)}. \quad (16)$$

Here the first term corresponds to the correlation with velocity variation at the last time step and the second terms accounts for the random contribution of local fluctuating velocity. χ_i is a Gaussian random number with mean value zero and a standard deviation of unity. The correlation function, $R_{P,i}$, is the product of a Lagrangian and a Eulerian part, $R_{P,i}(\Delta t,\Delta r) = R_{L,i}(\Delta t)R_{E,i}(\Delta r)$. The Lagrangian correlation function takes an exponential form as

$$R_{L,i}(\Delta t) = \exp\left(-\frac{\Delta t}{T_L}\right), \quad (17)$$

and the Lagrangian integral time scale is computed as $T_\mathrm{L} = C_T\sigma^2/\tilde{\varepsilon}$ with $\sigma = \sqrt{2\tilde{k}/3}$ and C_T = 0.24 [17]. The Eulerian part can be expressed as functions of longitudinal and transversal correlation coefficients, $f(\Delta r)$ and $g(\Delta r)$ as

$$R_{E,i}(\Delta r) = \{f(\Delta r) - g(\Delta r)\}\frac{\Delta r_i \Delta r_j}{\Delta r^2} + g(\Delta r)\delta_{ij}, \quad (18)$$

and

$$f(\Delta r) = \exp\left(-\frac{\Delta r}{L_E}\right) \quad (19)$$

and

$$g(\Delta t) = \left(1 - \frac{\Delta r}{2L_E}\right)\exp\left(-\frac{\Delta r}{L_E}\right). \quad (20)$$

Here, $\Delta r = |\mathrm{u}\text{-}\mathrm{v}_d|\Delta t$ is the separation distance between the fluid element and the droplet, and the integral length scale is $L_E = 3.0T_L\sigma$. For simplicity, in the results and discussion sections, these two models will be referred to as 'ELT' and 'LEM' models, respectively.

The present study concerns one-component sprays with pure fuel acetone in air. The droplet evaporation is described through the droplet mass evaporation rate, $\dot{m}_d$, as [20]

$$\dot{m}_\mathrm{d} = 2\pi r_\mathrm{d}\hat{\rho}\hat{D}\widetilde{\mathrm{Sh}}\ln(1 + B_\mathrm{M}), \quad (21)$$

where the hat denotes properties in the surrounding gas film, which are determined using the "1/3 -rule" [18], and B_M is the mass transfer number, $B_\mathrm{M} = (Y_\mathrm{Fs}\text{-}Y_\infty)/(1\text{-}Y_\mathrm{Fs})$, where Y_∞ denotes the mass fraction of fuel in the surrounding gas phase.

The droplet heating is calculated using the infinite conductivity model for acetone with its low boiling temperature as [19]

$$\frac{dT_\mathrm{d}}{dt} = \frac{f_2}{3\tau_\mathrm{d}} \frac{\widetilde{\mathrm{Nu}}}{\mathrm{Pr_g}} \left(\frac{C_{p,\mathrm{g}}}{C_{p,l}}\right)(T_\mathrm{g} - T_\mathrm{d}) - \frac{L_V(T_\mathrm{d})}{C_{p,l}} \left(\frac{\dot{m}_\mathrm{d}}{m_\mathrm{d}}\right). \quad (22)$$

$\tau_\mathrm{d} = 2/9\rho_l r_\mathrm{d}^2/\mu_\mathrm{g}$ is the droplet relaxation time, and μ_g the gas viscosity around the droplet. $C_{p,\mathrm{g}}$ and $C_{p,l}$ are the heat capacity of gas and liquid phase, respectively, and $L_\mathrm{V}(T_\mathrm{d})$ the temperature dependent latent heat of vaporization. The droplet mass, m_d is $m_\mathrm{d} = 4/3\pi\rho_l r_\mathrm{d}^3$. f_2 is a correction factor for the heat transfer due to evaporation discussed below.

Following the work of Abramzon and Sirignano [20], the modified Nusselt $\widetilde{\mathrm{Nu}}$ and Sherwood numbers $\widetilde{\mathrm{Sh}}$ are substituted in Eqs. (21)-(22). This modification is used to account for the blowing effect on the droplet evaporation. The modified Nusselt and Sherwood numbers yield [20]

$$\widetilde{\mathrm{Nu}} = 2 + \frac{\mathrm{Nu} - 2}{F(B_\mathrm{T})} \quad (23)$$

$$\widetilde{\mathrm{Sh}} = 2 + \frac{\mathrm{Sh} - 2}{F(B_\mathrm{M})}, \quad (24)$$

with

$$F(B) = \frac{(1+B)^{0.7}}{B} \ln(1+\mathrm{B}). \quad (25)$$

In Eq. (25), B stands for either the Spalding mass or heat transfer number, $B_\mathrm{T} = (1+B_\mathrm{M})^{\phi}$-1 and $\phi = (1/\mathrm{Le})(C_{p,l}/C_{p,\mathrm{g}})(\widetilde{\mathrm{Sh}} / \widetilde{\mathrm{Nu}})$ [20].

For the case of thermodynamic equilibrium, the mole fraction at the droplet surface, $\mathrm{X_{Fs,eq}}$ is computed by the Clausius-Clapeyron equation [21]

$$X_\mathrm{Fs,eq} = \exp\left[\frac{L_V(T_\mathrm{d})W_\mathrm{vap}}{\mathrm{R}}\left(\frac{1}{T_\mathrm{B}} - \frac{1}{T_\mathrm{d}}\right)\right], \quad (26)$$

where W_vap is the vapor molecular weight, R is the universal gas constant, and T_B and T_d are the boiling and the droplet temperature, respectively.

Miller et al. [19] compared several liquid droplet evaporation models in many-droplet gas liquid flows, and the results show the improved performance of non-equilibrium models especially for small droplets and moderate or large evaporation rate cases, which can be expected in the present polydisperse sprays. Based on the Langmuir-Knudsen law [19], the thermodynamic non-equilibrium effects at the gas/droplet interface is considered in this work, where a deviation term is added to the equilibrium surface mole fraction, $X_\mathrm{Fs,eq}$ [19]

$$X_\mathrm{Fs,neq} = X_\mathrm{Fs,eq} - \left(\frac{L_K\beta}{r_\mathrm{d}}\right). \quad (27)$$

L_K is the Knudsen layer thickness [19],

$$L_K = \frac{\mu_\mathrm{g}\sqrt{2\pi T_\mathrm{d}\mathrm{R}/W_\mathrm{vap}}}{p_\mathrm{g}\mathrm{Sc_g}}, \quad (28)$$

where p_g is the pressure of the gas phase, and β is a non-dimensional evaporation parameter [19]

$$\beta = 1.5\,\mathrm{Pr_g}\tau_\mathrm{d}\frac{\dot{m}_\mathrm{d}}{m_\mathrm{d}}. \quad (29)$$

For the non-equilibrium model, $f_2 = \beta/(e^\beta - 1)$ [19], which enters Eq. (22) and acts as a correction factor of the Nusselt number.

With the above formulations of the droplet dynamics, the spray source terms for mass, S_v, momentum, $\boldsymbol{S}_\mathrm{m}$, and energy, S_e, can be estimated [3, 11].

$$S_\mathrm{v} = \sum_{k=1}^{n_\mathrm{d}} N_{\mathrm{d},k}\,\dot{m}_\mathrm{d}, \quad (30)$$

$$\boldsymbol{S}_\mathrm{m} = \sum_{k=1}^{n_\mathrm{d}} N_{\mathrm{d},k}\left[-m_\mathrm{d}\frac{\mathrm{d}\mathbf{V}_{\mathrm{d},k}}{\mathrm{d}t} + \dot{m}_\mathrm{d}\mathbf{V}_{\mathrm{d},k}\right] \quad (31)$$

and

$$S_\mathrm{e} = \sum_{k=1}^{n_\mathrm{d}} N_{\mathrm{d},k}\,\dot{m}_\mathrm{d} h_\mathrm{d}. \quad (32)$$

The summation is applied over the number of droplet parcels, n_d that pass through a computational grid cell, and $N_{\mathrm{d},k}$ is the number of real droplets in the computational parcel k.

The spray evolution in the continuous gas phase is described with the representative droplet parcels, where each computational parcel contains a number of droplets with identical location, size, velocity and temperature. The temporal evolution of the particles' characteristics, which are governed by Eqs. (11)-(22), are recorded through a Lagrangian particle tracking method [11]. At the inlet boundary, the liquid particles are injected with prescribed initial values and tracked until they reach the exit boundary or are completed vaporized. Only dilute gas-particle flows are considered in this work, so that particle-particle interactions are neglected whereas the two-way coupling is retained and the effect of evaporating droplets on the carrier gas phase is accounted through the source terms defined in Eqs. (30-32).

For the carrier gas phase, the closed system of equations is formed by applying a joint PDF method in a Eulerian CFD solver. The solution of gas phase PDF in the velocity and mixture fraction space is achieved by numerical integration of the SDEs (3) - (4) for notional gas particles. The averaged mean variables appearing in the PDF model are computed by solving the conservation equations of mass, momentum and enthalpy of the gas phase, cf. Eqs. (5)–(9), which are solved by a two-dimensional finite-volume CFD solver based on SIMPLE algorithm, and a relaxation method is used to enhance the computational stability and accelerate the convergence [11].

Results and Discussion

Two poly-disperse turbulent acetone spray flows in air are studied using the model described above. As shown in Fig. 1, the spray burner is composed of a central jet nozzle with diameter D = 10.5 mm and a surrounding co-flow air stream with a diameter of 104 mm [1]. This co-flow burner assembly is mounted in a wind tunnel with bulk velocity of 4.5 m/s. The liquid acetone is injected 215 mm upstream of the nozzle exit plane, leading to partial evaporation of droplets before reaching the exit plane and a mixture of acetone and air is found at the nozzle inlet. The flow rates of different streams at the inlet boundary for two sprays are listed in Table 1. Compared with SP2, SP6 has a lower liquid mass flow-rate but the same carrier air flow rate. These data correspond to the experimental set B of the SP2 and SP6 acetone evaporating spray jets [1]. In the following section, the comparison between the computed and experimental data at different cross-sections is made for the main droplet properties, i.e. Sauter mean diameter, droplet volume flux, and droplet axial and radial mean and fluctuating velocities.

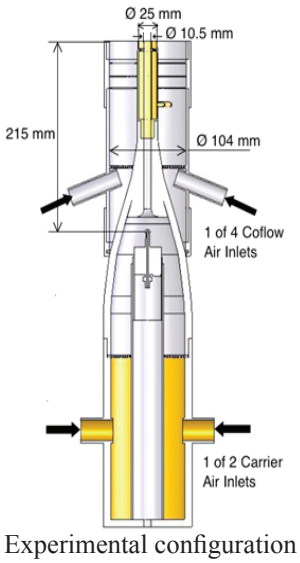

Fig. 1. Experimental configuration [1].

Table 1
Inflow conditions of the acetone sprays SP2 and SP6 [1]

Parameter	SP2	SP6
Carrier mass flow rate (g/min)	225	225
Liquid fuel injection rate (g/min)	75	45
Measured liquid fuel rate at inlet (g/min)	33.9	26.7
Vapor fuel rate at inlet (g/min)	41	18.3
Jet Reynolds number	31.800	28.100

The numerical convergence and accuracy of Eulerian-Lagrangian simulations of two-phase flows have been discussed in many studies [22, 23] A higher number of particles per cell is required for an accurate estimation of the interphase momentum transfer term. In the present computation, the sensitivity of computed droplet mean properties to the initial number of droplet trajectories at the inlet were tested in the range of 5,000 to 20,000, and a total number of 10,000 parcels with constant statistical weight is found to be suitable. To generate the inlet profiles for the computations, the profiles at the first experimental cross section are used. First, the particles' position is determined randomly with a normal distribution around each measurement position, and the droplet size is prescribed assuming a Rosin-Rammler distribution [17], matching the measured Sauter mean diameter (SMD) of the spray. The droplet velocity is pre-scribed using a Gaussian distribution matching the experimental mean and fluctuating velocities of the corresponding droplet size groups [7]. The gas phase velocity and its turbulence intensity at the inlet plane are taken from the experiment. As shown in Tab. 1, for both sprays considered here pre-vaporized fuel vapor is found at the nozzle exit and causes a non-zero mixture fraction at the inlet. This air-fuel mixture retards droplets evaporation because of the decreased mass transfer coefficient. Based on the mass flow rate of air and vapor fuel, the inlet mixture fraction is set to be 0.154 and 0.0752 for SP2 and SP6, respectively. The thermo-properties of liquid acetone are taken from Perry et al. [24].

Figure 2 shows radial profiles of Sauter mean diameter computed using two different dispersion models (ELT and LEM) in the comparison with the measurements (Exp.) at four cross-sections x/D = 5, 10, 20, 30. It is seen that generally, good agreement between the computed SMD profiles and the experimental data is achieved especially upstream, and the computed results tend to underpredict the SMD near the centerline downstream

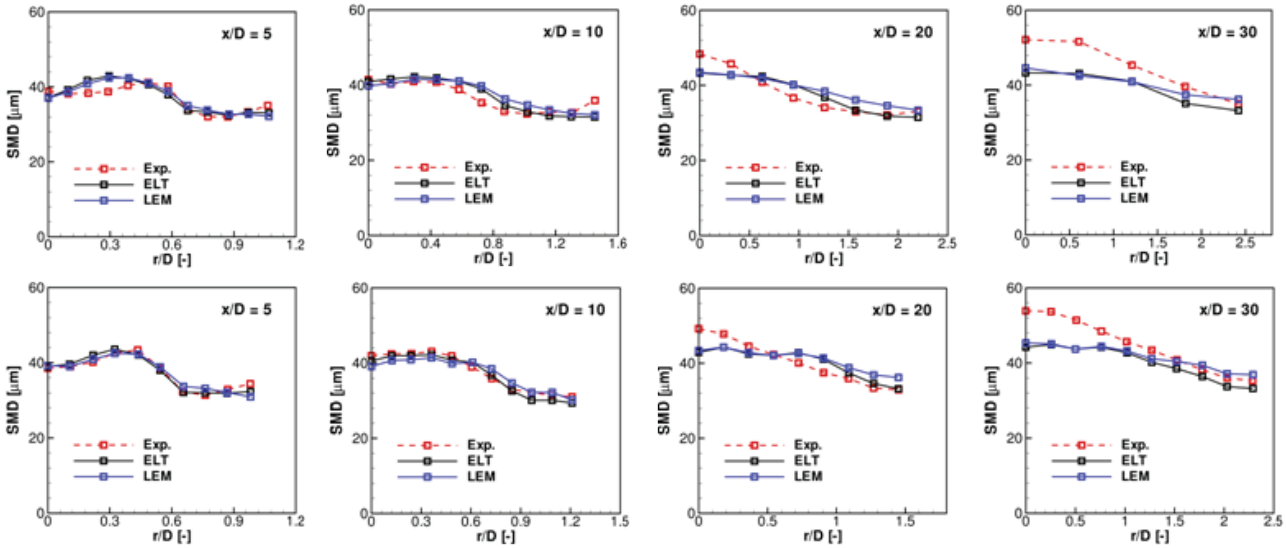

Fig. 2. Radial profiles of the Sauter mean diameter, SMD, in sprays SP2 (top) and SP6 (bottom).

the nozzle exit. The discrepancies between the two dispersion models are similar in these two spray flows, and with the single-step Langevin equation model (LEM), the predicted SMD is little smaller near the inner jet, but larger towards the edge of the spray, which is much more pronounced at higher distances from the nozzle exit. This comes from the fact that in particle-laden jet flows, the effect of the turbulent dispersion is mainly reflected by the radial dispersion of the droplets. The profiles of the SMD show that the jet is broadened further downstream. In this sense, the turbulent dispersion model LEM causes a more pronounced radial dispersion of droplets compared to the ELT model. The comparison of the droplet volume flux predictions with the two dispersion models is shown in Fig. 3. At x/D = 5, the computed radial profiles match reasonably well with the experimental data, whereas from cross-section x/D = 10 downwards, the numerical results over-predict the liquid volume fluxes near the centerline, and this becomes even more obvious at cross-sections x/D = 20 and 30. This shows an accumulation tendency of droplets towards the centerline while moving downstream. This observation has also been reported in other discrete droplet calculations [25]. Moreover, as indicated in the computed radial profiles of SMD, the LEM model gives a lower spray volume flux near the centerline due to the more intense radial droplet dispersion.

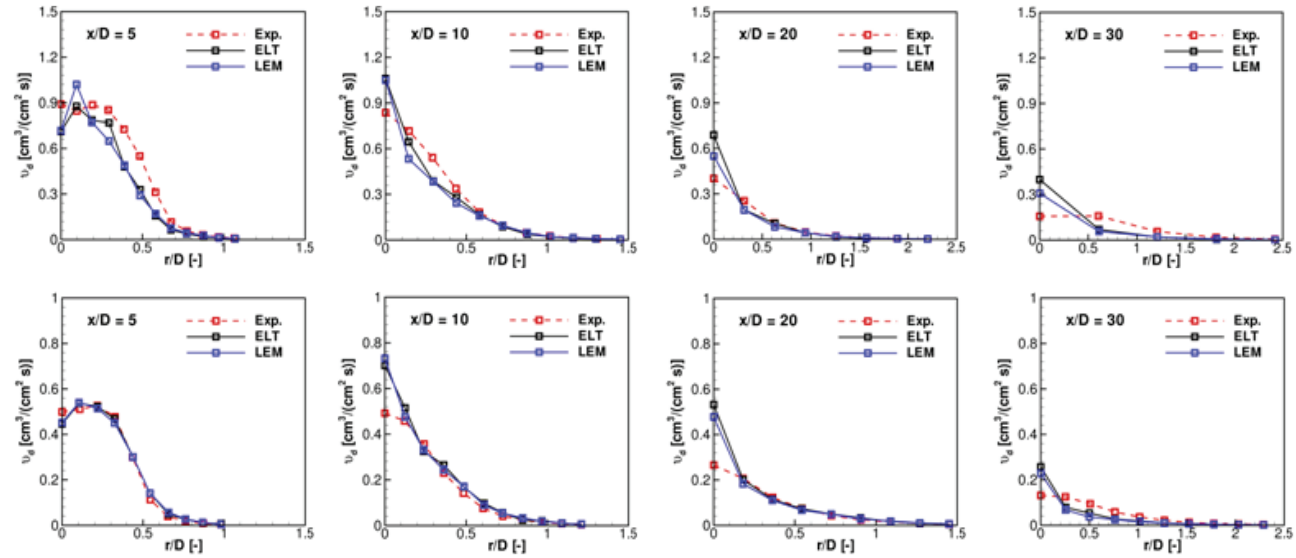

Fig. 3. Radial profiles of droplet volume flux. SP2 (top) and SP6 (bottom).

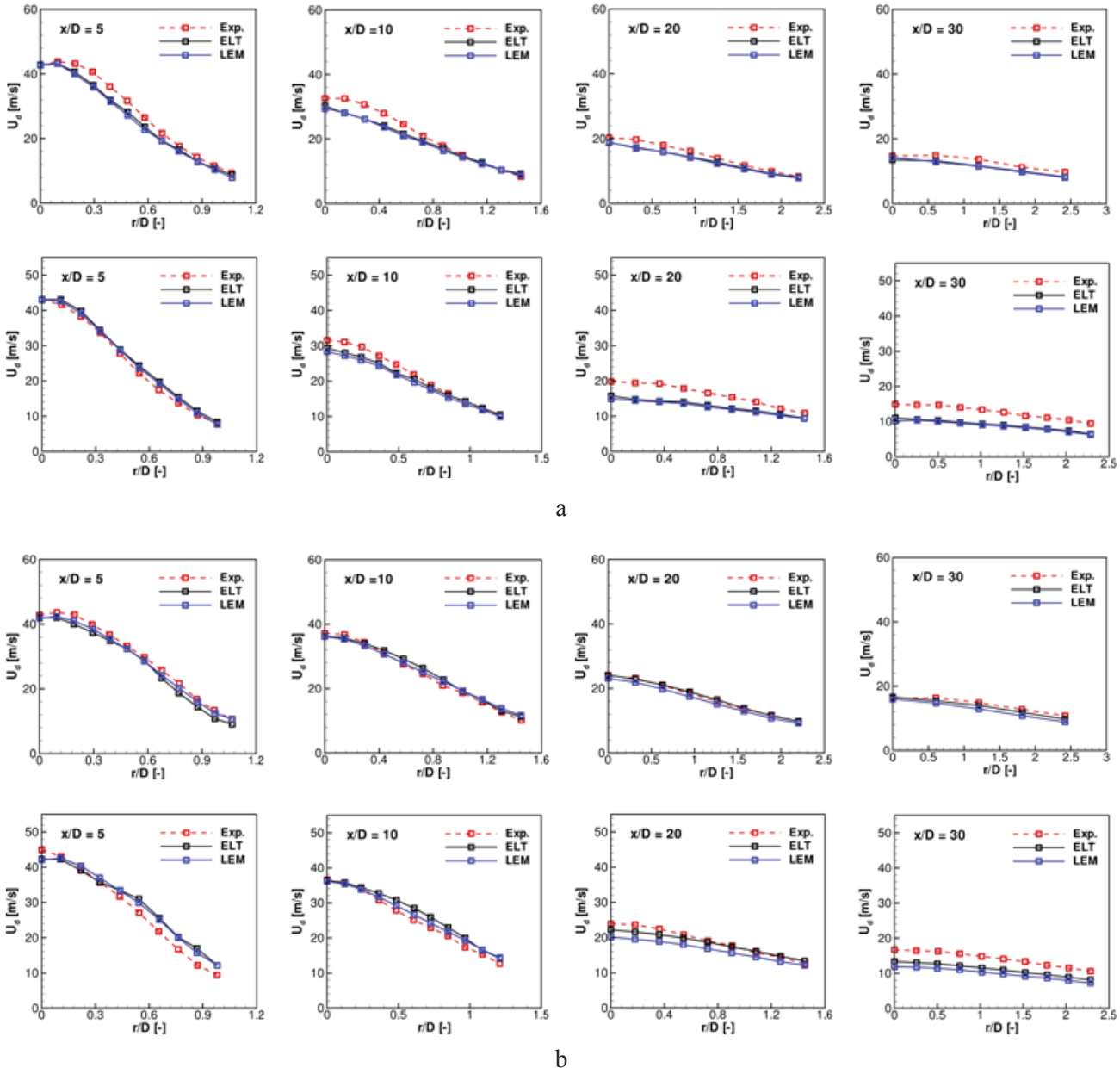

Fig. 4. Radial profiles of the mean axial droplet velocity for different size classes (a): $0 < d_d \leq 10$ μm, (b): 40 μm $< d_d \leq 50$ μm. SP2 (top), SP6 (bottom).

Figure 4 presents the radial profiles of the axial mean velocity of droplets conditioned on size class (a): $0 < d_d \leq 10$ μm and (b): 40 μm $< d_d \leq 50$ μm at different cross-sections. In Figs. 4(a) and 4(b), the top part refers to SP2 and the bottom corresponds to SP6. The computed profiles generally follow a similar trend as the measured data, and the comparison shows that in contrast to the small droplets' behavior, the mean velocity of the larger droplets changes with different dispersion models, where the LEM model predicts lower values.

The corresponding computed profiles of the droplet fluctuating velocity are depicted in Fig. 5. For the droplet size class $0 < d_d \leq 10$ μm, the fluctuating velocity is augmented using the dispersion model LEM, whereas for the larger droplets, at $x/D = 5$, the peak value of the axial fluctuation velocity is smaller but closer to the measured profiles. In Fig. 5 (a), at $x/D = 5$, the experimental data show peak values at about r/D = 0.4-0.6 in both spray flows, which can be considered as the locations with intense turbulence mixing or positions where

the production of the turbulent kinetic energy of the gas phase is highest. The peak value is not well predicted by the computation, and small droplets less than 10 μm act as track particles, which essentially follow the gas phase. In this sense, the gas phase turbulence intensity is under-predicted, and this then results in the under-estimation of the droplet radial mean velocity as shown in Fig. 6.

Computed droplet radial mean velocity profiles and corresponding fluctuations in two spray flows are shown in Figs. 6 and 7. Similar to the axial mean velocity, no big difference between the two dispersion models LEM and ELT is found in the prediction of radial mean velocity. In contrast, the radial velocity fluctuations predicted by LEM model is higher and they is closer to the experiment; larger droplets are more sensitive to the different dispersion models.

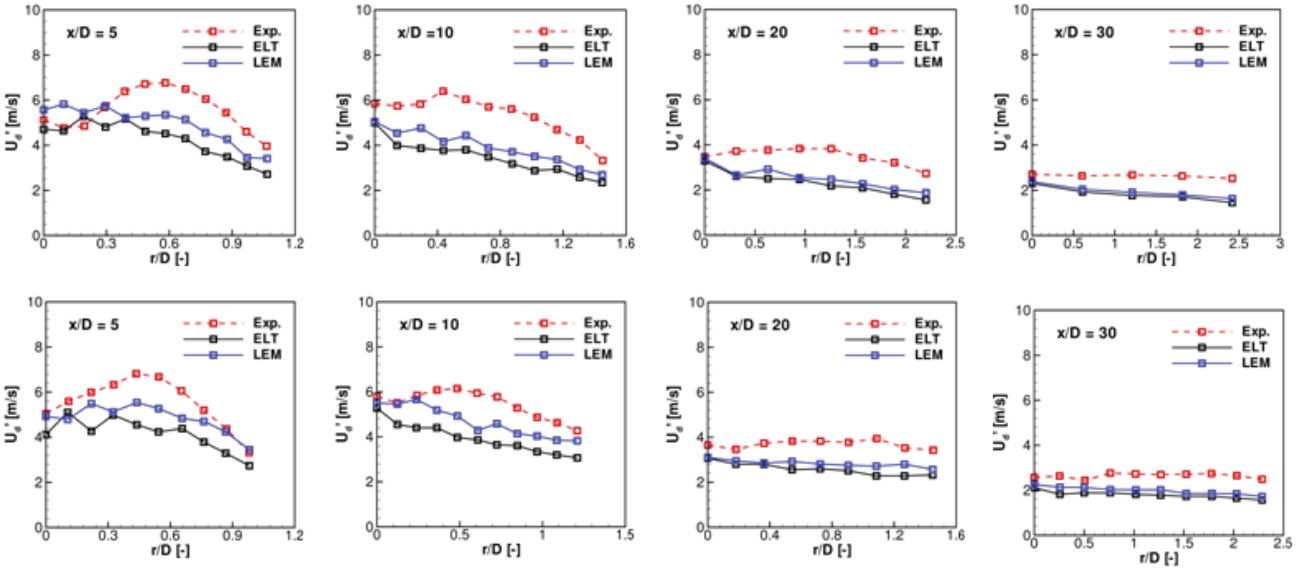

a

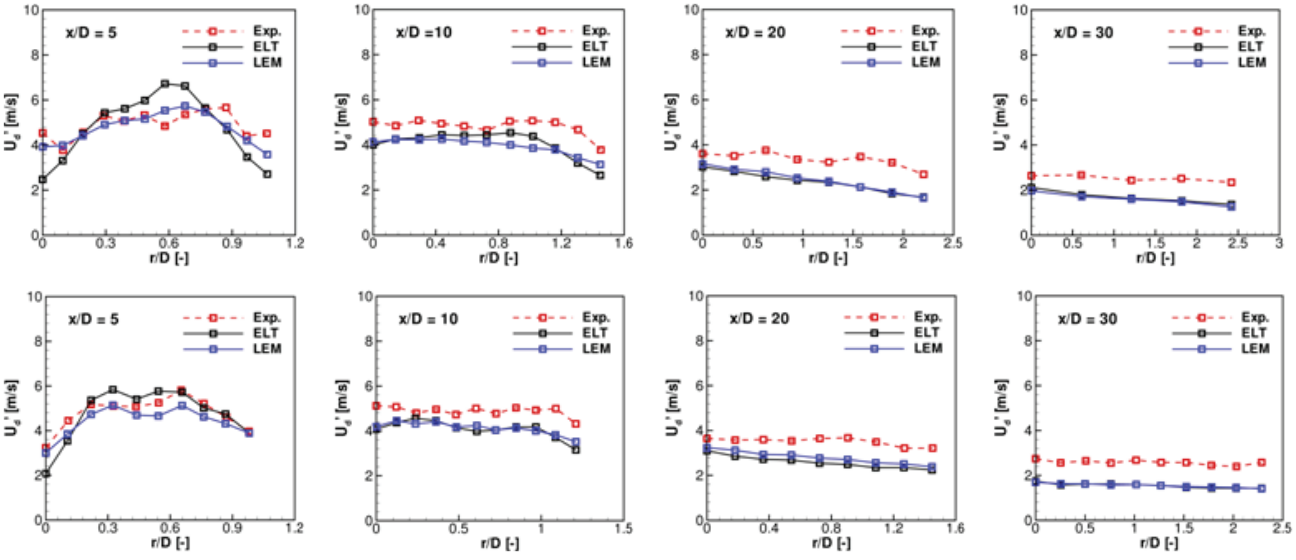

b

Fig. 5. Radial profiles of the axial fluctuating droplet velocity for different size classes (a): $0 < d_d \leq 10$ μm, (b): 40 μm $< d_d \leq 50$ μm. SP2 (top), SP6 (bottom).

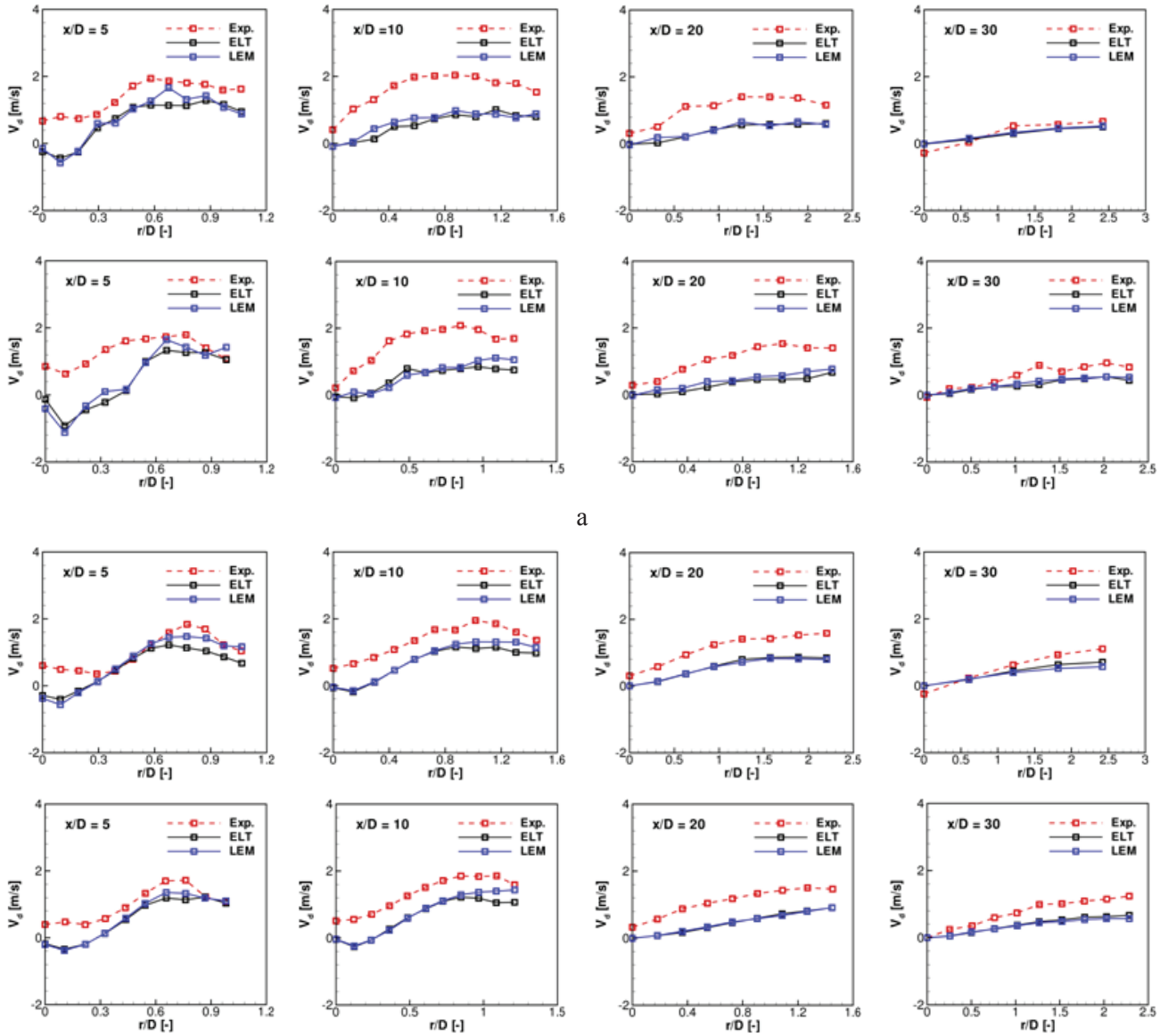

Fig. 6. Radial profiles of the mean radial droplet velocity for different size classes (a): $0 < d_d \leq 10$ μm, (b): 40 μm $< d_d \leq$ 50 μm. SP2 (top), SP6 (bottom).

Conclusion

In the present study, a Eulerian-Lagrangian approach is employed to simulate two droplet-laden two-phase turbulent flows. The approach is based on a statistical description of continuous gas phase with the joint gas velocity and mixture fraction probability density function, coupled with the Eulerian finite-volume method providing the necessary information of the turbulence and mean velocity and pressure field. The spray evolution is described using a Lagrangian discrete parcel method. The transported joint PDF equation is solved using a Lagrangian Monte-Carlo method. The simplified Langevin model and the interaction-by-exchange-with-the-mean (IEM) model are used for the velocity and scalar evolution of discrete gas particles. For the disperse phase, two droplet dispersion models are compared and evaluated, and the LEM (the one-step Langevin equation model) leads to larger droplet fluctuating velocities and radial dispersion of droplets. Generally, an overall good agreement between computation and experiment for droplet size and mean velocity is reported.

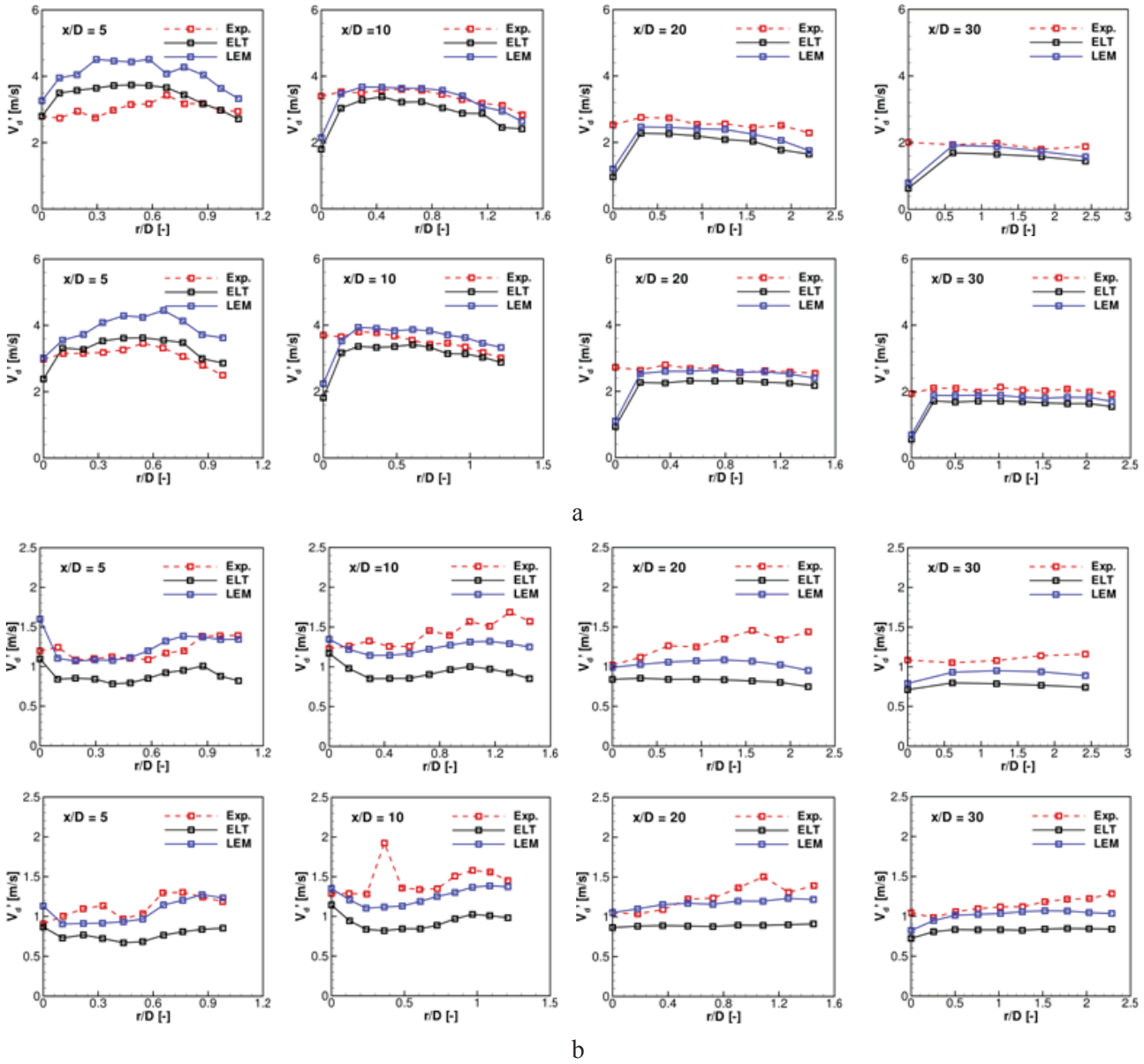

Fig. 7. Radial profiles of the radial fluctuating droplet velocity for different size classes (a): $0 < d_d \leq 10$ µm, (b): 40 µm $< d_d \leq 50$ µm. SP2 (top), SP6 (bottom).

Acknowledgment

Y. Hu acknowledges financial support through CSC.

References

[1]. J.D. Gounder, A. Kourmatzis, and A.R. Masri, Combust. Flame 159 (11) (2012) 3372–3397.
[2]. R. Fox, Annu. Rev. Fluid Mech., 44 (2012) 47–76.
[3]. H.-W. Ge, and E. Gutheil, Atomization and Sprays, 16 (5) (2006) 531–542.
[4]. B. Merci, and E. Gutheil, Experiments and Numerical Simulations of Turbulent Combustion of Diluted Sprays. Springer, Heidelberg, 2014.
[5]. A.R. Masri, and J.D. Gounder, "Details and complexities of boundary conditions in turbulent piloted dilute spray jets and flames". In Experiments and Numerical Simulations of Diluted Spray Turbulent Combustion, Merci, B., Roekaerts, D., and Sadiki, A., Eds., Springer, Heidelberg, 2011.
[6]. M. Chrigui, J. Gounder, A. Sadiki, A.R. Masri, and J. Janicka, Combust. Flame 159 (8) (2012) 2718–2741.

[7]. S. De, and S.H. Kim, Combust. Flame 160 (10) (2013) 2048–2066.
[8]. C. Heye, V. Raman, and A.R. Masri, Proc. Combust. Inst. 34 (1) (2013) 1633–1641.
[9]. H.-W. Ge, Y. Hu, and E. Gutheil, Combust. Sci. Technol. 184(10-11) (2012) 1664–1679.
[10]. R.M. Humza, Y. Hu, and E. Gutheil, "Probability density function modeling of turbulent spray combustion". In Experiments and Numerical Simulations of Turbulent Combustion of Diluted Sprays. B. Merci and E. Gutheil, Eds., Springer, Heidelberg, 2014.
[11]. C. Hollmann, and E. Gutheil, Proc. Combust. Inst. 26 (1996) 1731–1738.
[12]. S.B. Pope, Prog. Energy Combust. Sci. 11 (2) (1985) 119–192.
[13]. H.-W. Ge, and E. Gutheil, Combust. Flame 153 (12) (2008) 173–185.
[14]. L. Schiller, and A.Z. Naumann, "Über die grundlegenden Berechnungen bei der Schwerkraftaufbereitung". Verein Deutscher Ingenieure 77 (1933) 318–320.
[15]. A.D. Gosman, and E. Ioannides, Journal of Energy 7 (1983) 482–490.
[16]. S. Laín, and M. Sommerfeld, Powder Technol. 184 (1) (2008) 76–88.
[17]. C. Crowe, J.D. Schwarzkopf, M. Sommerfeld, and Y. Tsuji, Multiphase flows with droplets and particles, Second Edition. CRC Press, Boca Raton, Florida, 2011.
[18]. G. Hubbard, V. Denny, and A. Mills, Int. J. Heat Mass Transfer, 18 (9) (1975) 1003–1008 (1975).
[19]. R. Miller, K. Harstad, and J. Bellan, Int. J. Multiphase Flow 24 (6) (1998) 1025–1055.
[20]. B. Abramzon, and W. Sirignano, Int. J. Heat Mass Transfer 32 (9) (1989) 1605–1618 .
[21]. B.E. Poling, J.M. Prausnitz, and J.P. O'Connell, Properties of Gases and Liquids, Fifth Edition. McGraw-Hill, 2001.
[22]. R. Garg, C. Narayanan, and S. Subramaniam, Int. J. Multiphase Flow 35 (4) (2009) 376–388.
[23]. R. Garg, C. Narayanan, D. Lakehal, and S. Subramaniam, Int. J. Multiphase Flow 33 (12) (2007) 1337–1364.
[24]. D.W. Green, and R.H. Perry, Perry's chemical engineers' handbook, Eighth Edition. McGraw-Hill, 2007.
[25]. X.-Q. Chen, and J.C. Pereira, Numer. Heat Transfer, Part A, 27 (2) (1995) 143–162.

Received 25 March 2014